A Biparatopic Antibody–Drug Conjugate to Treat MET-Expressing Cancers, Including Those that Are Unresponsive to MET Pathway Blockade

John O. DaSilva, Katie Yang, Oliver Surriga, Thomas Nittoli, Arthur Kunz, Matthew C. Franklin, Frank J. Delfino, Shu Mao, Feng Zhao, Jason T. Giurleo, Marcus P. Kelly, Sosina Makonnen, Carlos Hickey, Pamela Krueger, Randi Foster, Zhaoyuan Chen, Marc W. Retter, Rabih Slim, Tara M. Young, William C. Olson, Gavin Thurston, and Christopher Daly

ABSTRACT

Lung cancers harboring mesenchymal-to-epithelial transition factor (*MET*) genetic alterations, such as exon 14 skipping mutations or high-level gene amplification, respond well to MET-selective tyrosine kinase inhibitors (TKI). However, these agents benefit a relatively small group of patients (4%–5% of lung cancers), and acquired resistance limits response durability. An antibody–drug conjugate (ADC) targeting MET might enable effective treatment of MET-overexpressing tumors (approximately 25% of lung cancers) that do not respond to MET targeted therapies. Using a protease-cleavable linker, we conjugated a biparatopic METxMET antibody to a maytansinoid payload to generate a MET ADC (METxMET-M114). METxMET-M114 promotes substantial and durable tumor regression in xenografts with moderate to high MET expression, including models that exhibit innate or acquired resistance to MET blockers. Positron emission tomography (PET) studies show that tumor uptake of radiolabeled METxMET antibody correlates with MET expression levels and METxMET-M114 efficacy. In a cynomolgus monkey toxicology study, METxMET-M114 was well tolerated at a dose that provides circulating drug concentrations that are sufficient for maximal antitumor activity in mouse models. Our findings suggest that METxMET-M114, which takes advantage of the unique trafficking properties of our METxMET antibody, is a promising candidate for the treatment of MET-overexpressing tumors, with the potential to address some of the limitations faced by the MET function blockers currently in clinical use.

Introduction

Human cancers that harbor either *MET* exon 14 skipping mutations (*MET*-ex14) or *MET* gene amplification are dependent on MET signaling for growth and survival (1–3). Recent clinical trials demonstrate that MET-selective TKIs achieve high response rates in the *MET*-ex14 population, particularly in previously-untreated patients (4–6). As a result, capmatinib has been granted accelerated approval by the FDA for the treatment of patients *with MET*-ex14 non–small cell lung cancer NSCLC. Furthermore, responses to capmatinib have also been observed in *MET*-amplified cancers, although responsiveness appears to be limited to tumors with a *MET* gene copy number of at least 10 (5). Finally, *EGFR*-mutant lung cancers that have progressed on EGFR TKIs and that harbor *MET* amplification have shown promising responses to combinations of EGFR plus MET inhibitors (7–9).

Although MET-selective TKIs exhibit impressive efficacy, *MET* genetic alterations are present in only 4%–5% of NSCLC (1, 2), limiting the population of patients in which blockade of MET signaling is likely to be effective. However, given that MET is overexpressed in a significant fraction of lung (25%–50%) and gastroesophageal cancers (10–13), targeting MET with an ADC is an attractive approach. Furthermore, the clinical benefit provided by MET-selective TKIs is likely to be limited by both inherent and acquired resistance, mediated by on-target alterations in the *MET* kinase domain as well as off-target alterations in drivers such as KRAS and EGFR (14–18). Importantly, the efficacy of a MET ADC is unlikely to be limited by either of these types of resistance. In addition, in settings of tumor resistance where a combination of targeted therapies might be called for, a MET ADC might be better tolerated than a combination of TKIs (e.g., EGFR plus MET), which can be associated with significant side effects.

While several MET ADCs are currently being evaluated in early-stage clinical trials (19–22), data are available for only one of these agents, telisotuzumab vedotin (ABBV-399), which has demonstrated a favorable safety profile and signs of antitumor activity in patients with NSCLC, although only a relatively small number of patients have been evaluated so far (20). Thus, it remains to be determined whether any of the MET ADCs that are currently being explored will provide significant benefit to cancer patients.

In this study, we conjugated our METxMET biparatopic antibody (23) to a novel maytansinoid payload (24) to generate the ADC METxMET-M114. The biparatopic antibody promotes efficient MET internalization and inhibits recycling, distinguishing it from conventional MET-targeting antibodies and making it an ideal candidate for an ADC approach. We show that METxMET-M114 promotes complete and sustained tumor regression in MET-overexpressing xenografts, including models that fail to respond to MET blockers because of either inherent lack of pathway dependence or acquired resistance. Importantly, METxMET-M114 demonstrated a favorable toxicity

Regeneron Pharmaceuticals, Inc., Tarrytown, New York.

Note: Supplementary data for this article are available at Molecular Cancer Therapeutics Online (http://mct.aacrjournals.org/).

Corresponding Author: John DaSilva, Regeneron Pharmaceuticals, 777 Old Saw Mill River Road, Tarrytown, NY 10591. Phone: 914-847-5392; E-mail: john.dasilva@regeneron.com

Mol Cancer Ther 2021;20:1966–76

doi: 10.1158/1535-7163.MCT-21-0009

profile in cynomolgus monkeys. Together, our findings indicate that METxMET-M114 is a promising candidate for the treatment of cancers that overexpress MET, with the potential to overcome some of the clinical challenges faced by MET pathway blockers.

Materials and Methods

Antibodies and reagents

Fully human antibodies against the MET extracellular domain were generated in VelocImmune mice using methods described previously (25, 26). The biparatopic METxMET antibody (Patent US2018/0134794A Example 5 (27)) was generated using methods described previously (28). To generate METxMET-M114 or -M1 (Patent US2018/0134794A Examples 21 and 22), METxMET antibody in 50 mmol/L HEPES, 150 mmol/L NaCl, pH 8.0, and 10–15% (v/v) DMA was conjugated with a 5–6 fold excess of SMCC-DM1 diastereomer or maytansin-3-N-methyl-L-alanine-N-Mebeta-alanine-carbamyl-(p-amino)benzyl-citrulline-valineadipoyl-succinate (M114). Excess payload was removed by molecular adsorption using activated charcoal. The conjugates were buffer exchanged into formulation buffer (PBS plus 5% glycerol), purified by size-exclusion chromatography or ultrafiltration and sterile filtered. Protein concentrations were determined by UV spectral analysis. Size-exclusion HPLC established that all conjugates used were >90% monomeric, and RP-HPLC established that there was <1% unconjugated linker payload. All conjugated antibodies were analyzed by UV for linker-payload loading values according to (29) and/or by mass difference, native versus conjugated.

An in-house version of the MET antibody ABT-700 (Patent US8,545,839 B2) was generated using the published primary sequences and produced in CHO-K1 cells. To generate an in-house version of Telisotuzumab vedotin (Patent US2017/0348429 A1), our version of ABT-700 was partially reduced and alkylated by adding the payload stock solution (mc-VC-PAB-MMAE, 8 equivalents) and the reaction was quenched by adding 12 equivalents of N-Acetyl-Cysteine. The average drug:antibody ratio of the in-house version of Telisotuzumab vedotin was approximately 3.1, the same as the published value (21).

An in-house version of the EGFR antibody cetuximab (Patent US6,217,866 B1) was generated from the published primary sequences and produced in CHO-K1 cells at Regeneron. Capmatinib was obtained from Selleck Chemicals.

X-ray crystallography

To determine the tubulin-bound structure of our M24 payload, we grew crystals of porcine tubulin (Cytoskeleton, Inc.) in complex with RB3 stathmin-like domain and tubulin tyrosine ligase (GenScript), following the procedure described in (30). Large, single crystals were soaked in stabilizer solution containing M24 at 0.1 mg/mL and frozen in liquid nitrogen. The 2.2 Å synchrotron dataset was processed using HKL2000, with the free R cross-validation set of reflections copied from PDB code 4IHJ (30). The atomic coordinates of 4IHJ were used as a starting point for refinement. After one cycle of refinement against the M24 soak dataset, a very clear difference in electron density was observed for the bound maytansinoid derivative. M24 was built into this difference density, and adjacent amino acid side chains and waters were adjusted as needed. The complete structure was then refined further (Supplementary Table S1). Model building was done using Coot (31), and refinement using Refmac5 (32). Atomic coordinates have been deposited in the RCSB Protein Data Bank with PDB ID 7L05.

Analysis of tumor cell cytotoxicity and signaling

All human cancer cell lines used in the study were obtained from ATCC and authenticated by short tandem repeat profiling (IDEXX Bioresearch). Cells were incubated in the presence of serial dilutions (1.5 pmol/L to 100 nmol/L) of ADC, unconjugated antibodies, free M24 payload, or cell-permeable free payload M3. Following 7 days of treatment, cell viability was determined with the CellTiter-Glo 2.0 Cell Viability Assay or by measuring the reduction of the indicator dye alamarBlue (Invitrogen).

For detection of apoptosis, EBC1 cells were stained with Annexin V-conjugated to fluorescein isothiocyanate (FITC) and propidium iodide (PI) using the FITC Annexin V/Dead Cell apoptosis kit (Invitrogen V13242) according to the manufacturer's instructions. Immediately after staining, the cells were analyzed on a flow cytometer using 488-nm excitation and a 525-nm band pass filter for FITC and a 620-nm filter for PI detection. At least 10,000 cells were acquired in an Accuri C6 flow cytometer. Percentages of cells undergoing apoptosis were determined by dual-color analysis.

Cell lysates (50 mmol/L Tris pH7.4, 150 mmol/L NaCl, 0.25 mmol/L EDTA, 1% Triton) were resolved on 4%–20% Tris-Glycine gels and transferred to polyvinylidene difluoride membranes (Novex). The following antibodies were obtained from Cell Signaling Technologies and used for primary labeling of Western blots: MET (D1C2), Phospho-MET (Y1234/1235), Phospho-p44/42 MAPK (T202/Y204), β-tubulin. Secondary labeling was performed with horseradish peroxidase-conjugated antibody followed by chemiluminescence detection (GE Healthcare).

Tumor xenograft studies and IHC

All mouse experiments were conducted in accordance with the guidelines of the Regeneron Institutional Animal Care and Use Committee. Tumor cells (3×10^6 Hs746T cells or 5×10^6 EBC-1, NCI-H441, or NCI-H1975 cells) were implanted subcutaneously into the right flank of C.B.-17 SCID mice (6–8 weeks old). NSCLC patient-derived xenograft (PDX) fragments were implanted into the left flank of 5–8 week old female nude mice. Mice bearing established tumors were randomized ($n = 5$ to 6/group) such that the average tumor size and variance of the treatment groups were equivalent. Unconjugated antibodies were administered by subcutaneous injection once every 3–4 days. ADCs were administered by intravenous injection. Tumor volume was monitored with caliper measurements of length and width and was calculated as: $1/2 \times \text{length} \times \text{width}^2$.

Tumor samples were fixed in 10% buffered formalin, embedded in paraffin and sectioned (4 μmol/L). Immunohistochemistry was performed using anti-total c-Met (SP44) rabbit monoclonal primary antibody (Ventana Medical System). The staining was carried out according to the manufacturer's protocol on the Ventana Discovery XT platform utilizing the ultraView detection kit.

Immuno-PET imaging studies

METxMET and isotype control antibodies were incubated under basic conditions with a 3-fold molar excess of p-SCN-Bn-DFO (desferrioxamine) resulting in conjugates with an average DFO to antibody ratio of 1–1.5. Zirconium-89 (^{89}Zr) was chelated into the DFO-conjugated antibodies as described previously (33). Xenografts were established in male SCID mice and grown to 50–100 mm^3. Animals received a single intravenous injection of ^{89}Zr-radiolabeled control or METxMET antibody. For the 0.5 and 5.0 mg/kg groups, mice received 0.1 mg/kg ^{89}Zr- METxMET plus additional unlabeled METxMET antibody.

Sequential PET/CT images were acquired 6 days post-injection using a pre-calibrated G8 PET/CT instrument (Sofie Biosciences and Perkin Elmer). PET image was subsequently reconstructed using preconfigured settings. Decay-corrected PET data and CT data were processed using VivoQuant software (inviCRO Imaging Services) into false-colored coregistered PET-CT maximum intensity projections. Images were calibrated to indicate signal ranging from 0 to 30% of injected dose (ID) per volume, expressed as %ID/g.

Quantitative *ex vivo* biodistribution was performed on day 6 postinjection. Following terminal anesthesia, blood, tumors and normal tissues were collected. The ^{89}Zr γ-emission radioactivity of all samples at 511 keV was measured on an automatic gamma counter (Hidex AMG) and the weight of the blood and tissues was determined. The radioactivity in counts per minute relative to dose-standards was used to determine the %ID. The individual %ID/g value of each sample was determined by dividing the %ID by the respective sample weight.

Cynomolgus monkey study

The cynomolgus monkey study was conducted in accordance with IACUC guidelines. Cynomolgus monkeys (30 to 36 weeks old) were administered IgG4 control-M114 (2 animals/group) or METxMET-M114 (4 animals/group) diluted with 0.9% sodium chloride, USP (sterile saline) at 10 mg/kg via intermittent intravenous infusion on Days 1 and 22. Blood samples or tissues were collected at various time points for toxicokinetic analysis, clinical pathology and histopathology.

The concentrations of METxMET-M114 and IgG4 control-M114 in plasma were measured using the GyroLab xPlore platform. METxMET-M114 or IgG4 control-M114-specific biotinylated capture protein was added onto a Gyrolab Bioaffy 200 compact disc, which contained affinity columns preloaded with streptavidin-coated beads. Serial dilutions of standard and plasma samples were prepared in PBS + 0.5% BSA containing 0.67 to 2% NMS and added onto the columns. Captured human IgG was detected using an Alexa-647-conjugated mAb diluted in Rexxip F buffer. The resultant fluorescent signal was recorded in response units by the GyroLab xPlore instrument. Sample concentrations were determined by interpolation from a standard curve that was constructed using a 4-parameter logistic curve fit in Gyrolab Evaluator Software.

The concentration of M24 in plasma was determined using the Xevo TQ-S mass spectrometer. Experimental, standard (M24 in solution), and QC samples (M24 in solution mixed with untreated plasma and 2% v/v phosphoric acid) were mixed with 5:5:0.2 MeOH:H2O:H3PO4, centrifuged at 2,500 rpm for 10 minutes and loaded onto the elution plate (micro elution hydrophilic lipophilic balanced). Following two washes with 5% MeOH, samples and blanks were eluted with acetonitrile:MeOH:H2O 80:10:10 and subjected to mass spectrometry. Retention time and peak area were determined by Masslynx Mass Spectrometry software. Analyte concentrations were obtained from a calibration curve constructed by plotting peak area ratio versus concentration. Concentrations were calculated using linear regression with 1/x2 weighting.

Results

A biparatopic METxMET ADC promotes apoptosis of MET-overexpressing cancer cell lines irrespective of pathway dependence

To effectively target tumors that overexpress MET, we generated a MET ADC that employs our biparatopic METxMET antibody, in which each arm of the antibody recognizes a distinct, nonoverlapping epitope on the Sema domain of MET (23). Further, the METxMET antibody preferentially trafficks to lysosomes rather than recycling back to the cell surface and therefore promotes more effective degradation of MET than the parental antibodies. We conjugated the METxMET antibody to a novel maytansine derivative (24) to generate the MET ADC METxMET-M114. The cytotoxic payload (known as M24) was conjugated to antibody surface lysines using a protease-cleavable linker to generate an ADC with an average drug:antibody ratio of approximately 3.2 (**Fig. 1A**). To provide insight into the mode of action of M24, we determined its tubulin-bound structure by X-ray crystallography at 2.2-Å resolution (**Fig. 1B**). M24 binding to the tip of the α-tubulin subunit creates a bulky extrusion that inhibits the addition of tubulin subunits at the plus ends of growing microtubules. This mechanism of action is similar to that of other maytansines but distinct from microtubule-destabilizing agents such as vinca domain ligands, including MMAE and tubulysin, which introduce conformational changes at the interface between two tubulin dimers (34).

METxMET-M114 potently decreased the viability of EBC1 (*MET*-amplified NSCLC) and SNU5 (*MET*-amplified gastric cancer) cells, with EC_{50} values of 0.13 nmol/L and 0.07 nmol/L, respectively (**Fig. 1C**; Supplementary Table S2). Both of these cell lines express high levels of MET protein on their cell surface (Supplementary Table S3). Consistent with the mechanism of action of the cytotoxic payload, METxMET-M114 promoted apoptosis of these cell lines (**Fig. 1C**). As described previously, our unconjugated METxMET antibody also inhibits the growth of these MET-dependent cell lines (23), and promotes apoptosis (**Fig. 1C**). Thus, *MET*-amplified cancers can be treated effectively by either the unconjugated METxMET antibody or by METxMET-M114.

To explore the activity of METxMET-M114 in cell lines that are not dependent on the MET pathway, we tested its effect on the MET-overexpressing NSCLC cell lines NCI-H441 (low-level amplification) and NCI-H1975 (not *MET* amplified) (35, 36). METxMET-M114 reduced the viability of both cell lines, with EC_{50} values of 0.12 nmol/L (NCI-H441) and 2.59 nmol/L (NCI-H1975) (**Fig. 1D**; Supplementary Table S2). Importantly, METxMET-M114 did not decrease the viability of T47D breast cancer cells that lack MET expression, confirming the target dependence of cytotoxicity (T47D cells were killed by a cell-permeable variant of the free M24 payload, known as M3; **Fig. 1D**). Consistent with the lack of MET pathway dependence of NCI-H441 and NCI-H1975 cells, unconjugated METxMET antibody failed to promote apoptosis in these cell lines, while METxMET-M114 induced a significant degree of cell killing (**Fig. 1D**).

The ADC known as telisotuzumab vedotin is currently undergoing clinical evaluation in MET-expressing NSCLC (20). This ADC consists of the ABT-700 MET antibody conjugated to monomethyl auristatin E (MMAE) via a cathepsin-cleavable linker (21). We used the publicly available sequences of ABT-700 to produce an in-house version of that antibody, which was then conjugated to MMAE to generate a version of telisotuzumab vedotin that we refer to as Comp-MMAE. METxMET-M114 was in general more effective at killing both *MET*-amplified and -nonamplified cancer cells than Comp-MMAE (**Fig. 1C** and D; Supplementary Fig. S1). Thus, in terms of *in vitro* cytotoxicity, METxMET-M114 compares favorably to a clinical-stage ADC.

Recent studies have shown that some ADCs with noncleavable linkers, which release their linker-payload in lysosomes still bound to an amino acid from the antibody, require transporters (e.g., SLC46A3) for movement of the payload into the cytoplasm (37, 38). Interestingly, CRISPR-mediated knockout of SLC46A3 in NCI-H441 NSCLC cells had no effect on METxMET-M114 induced cytotoxicity (Supplementary Fig. S2). In contrast, SLC46A3 knockout completely abrogated

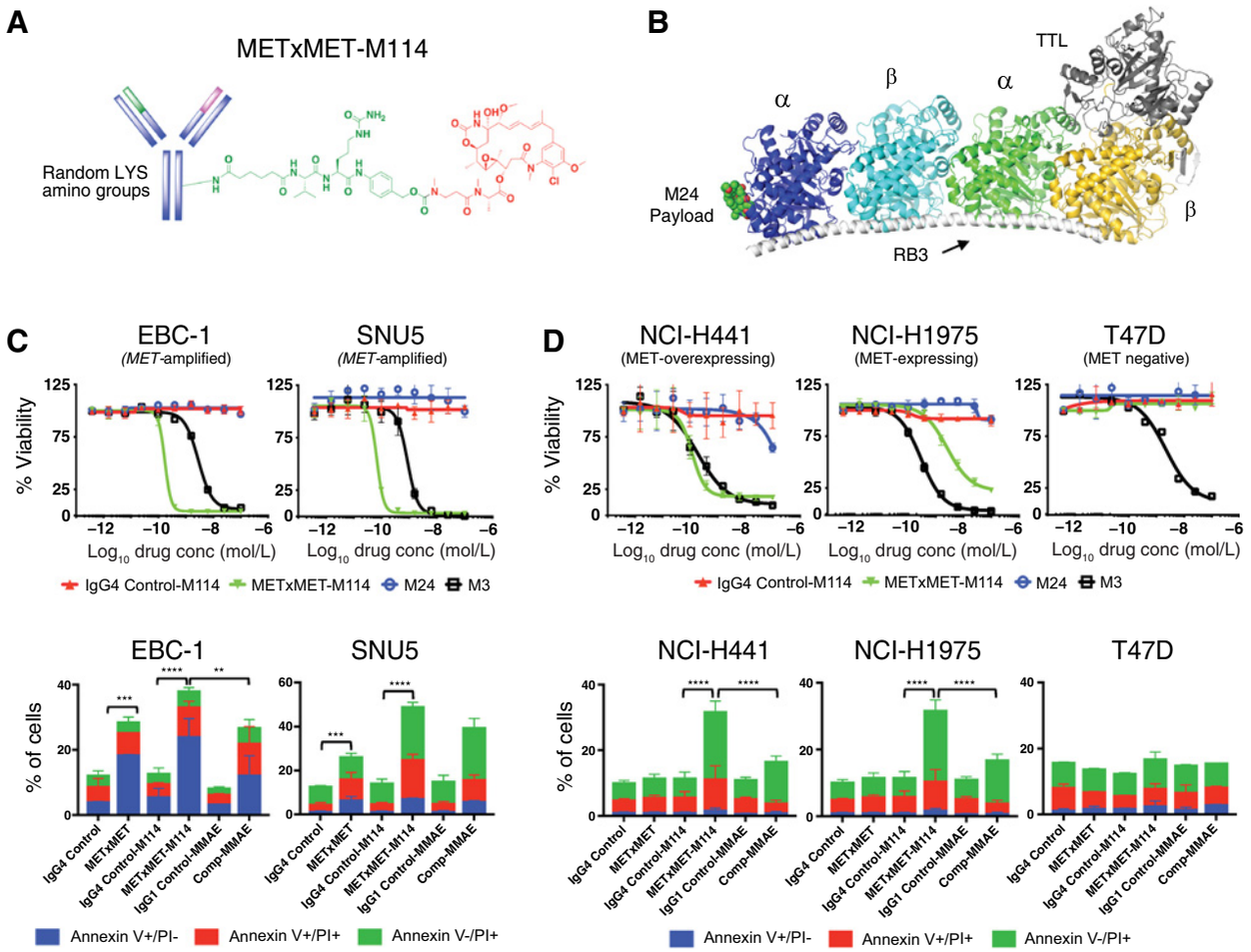

Figure 1.

A biparatopic METxMET ADC promotes apoptosis of MET-overexpressing cancer cell lines. **A,** Schematic of METxMET-M114, composed of a METxMET biparatopic antibody, a protease-cleavable linker, and the cytotoxic maytansine derivative M24. **B,** Ribbon representation of the tubulin–M24 complex, composed two αβ-tubulin, the stathmin-like protein RB3, and tubulin tyrosine ligase. **C** and **D,** Human EBC1, SNU5, NCI-H441, NCI-H1975, and T47D cells were incubated with the indicated antibodies, ADCs, cytotoxic free payload M24 or cell-permeable payload M3 at concentrations ranging from 1.5 pmol/L to 100 nmol/L. Cell viability was measured after 7 days of treatment. The line graphs depict the mean ± SD. To quantitate apoptosis, flow cytometric analysis was performed following 72 hours incubation with 10 nmol/L of the indicated antibodies or ADCs. Bar graphs depict the mean ± SD. **, $P < 0.005$; ***, $P < 0.0005$; ****, $P < 0.0001$, one-way ANOVA with Tukey *post hoc* test.

killing by a distinct METxMET ADC (METxMET-M1) that employs a maytansinoid payload and a noncleavable linker (providing a positive control for the genetic inactivation of SLC46A3). Thus, METxMET-M114 efficacy is not dependent on the SLC46A3 lysosomal transporter, perhaps because of linker cleavage and payload release in an earlier endocytic compartment.

METxMET ADC is highly effective in tumor models that overexpress MET

We next assessed the antitumor activity of our METxMET ADC in human tumors harboring *MET* genetic alterations. METxMET-M114 administered to mice at a dose of 2.5 mg/kg promoted substantial regression of *MET*-amplified EBC1 lung cancer xenografts and induced complete and durable tumor regression at doses greater than 5 mg/kg (**Fig. 2A**). In contrast, we have shown previously that a maximally effective dose (25 mg/kg) of unconjugated METxMET antibody results only in EBC1 tumor stasis, but no regression (23). This finding suggests the possibility that even in patients with lung cancer with *MET*-amplified tumors, a MET ADC approach may provide more benefit than a MET function–blocking approach.

In the *MET*-amplified and *MET*-ex14 Hs746T gastric cancer model, treatment with METxMET-M114 at 3 mg/kg induced tumor stasis and at 10 mg/kg provided complete, durable tumor regression (**Fig. 2B**). Although treatment with the unconjugated METxMET antibody also resulted in complete tumor regression, tumors escaped within several weeks, again highlighting the potential advantage of an ADC approach.

We next assessed the efficacy of METxMET-M114 in two NSCLC models, NCI-H441 and NCI-H1975, which overexpress MET in the absence of significant *MET* amplification. These tumors express lower levels of MET compared with *MET*-amplified Hs746T tumors, but do exhibit homogeneous plasma membrane expression of MET that is

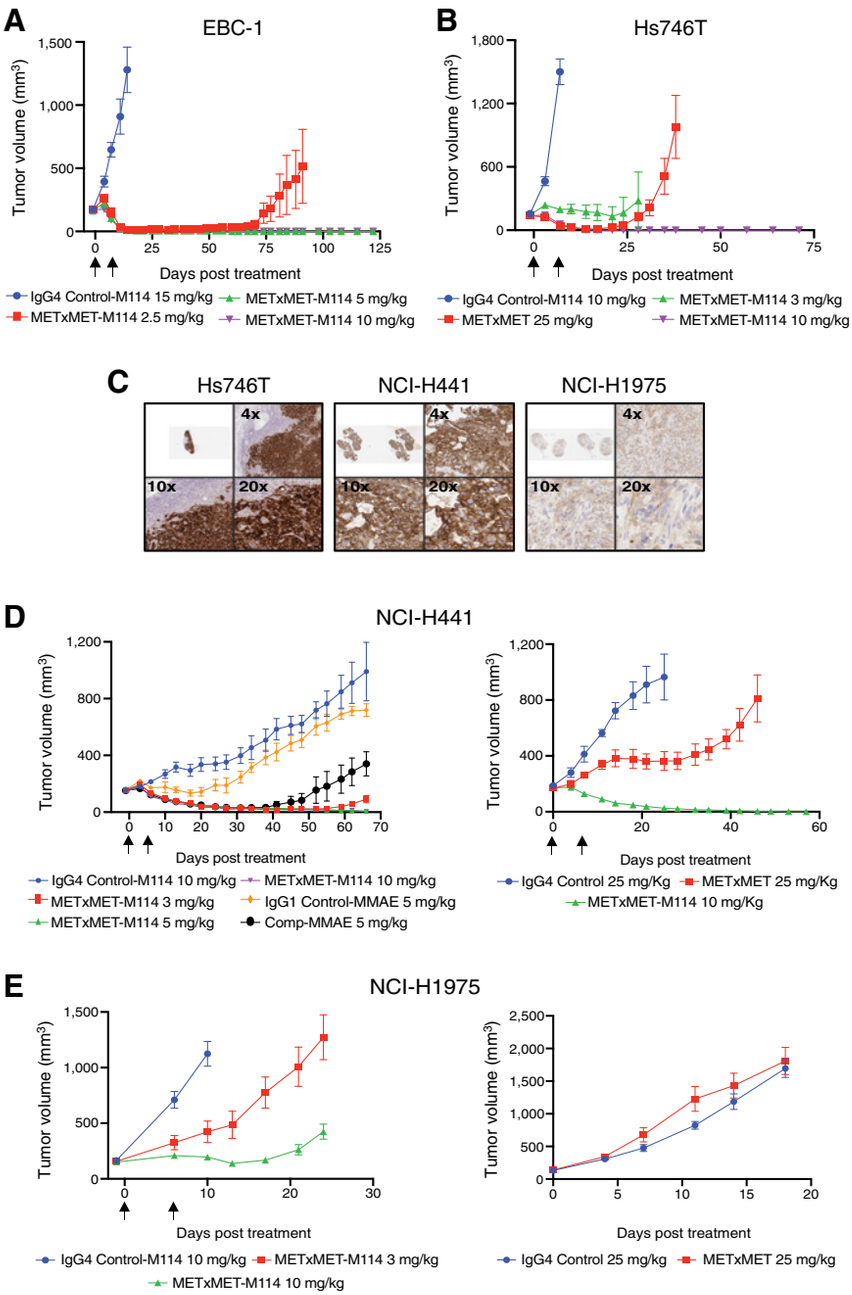

Figure 2.
METxMET ADC is highly effective in tumor models that overexpress MET. **A, B, D** and **E,** SCID mice bearing established tumors were randomized ($n = 5$ to 6/group) and treated with ADCs or unconjugated antibodies at the indicated doses. ADC administrations are indicated by arrows. Unconjugated METxMET antibody was administered twice per week. Line graphs depict the average tumor volumes ± SEM for each group. **C,** Immunohistochemical evaluation of Hs746T, NCI-H441, and NCI-H1975 tumor sections using SP44 MET antibody. The images depict the entire tumor sections or a field at 4x, 10x, or 20x magnification.

strong or moderate as determined by immunohistochemistry (**Fig. 2C**). METxMET-M114 at a dose of 3 mg/kg promoted complete but transient NCI-H441 tumor regression, achieving durable regression at doses of 5 mg/kg or higher (**Fig. 2D**). Blockade of MET signaling with the unconjugated METxMET antibody resulted only in delayed growth of NCI-H441 tumors, consistent with the general lack of pathway dependence in tumors without *MET* genetic alterations (**Fig. 2D**, right). In NCI-H1975 tumors, with moderate MET expression, METxMET-M114 administered at 10 mg/kg provided tumor stasis but no significant regression, whereas the unconjugated METxMET antibody had no effect on tumor growth (**Fig. 2E**). These results suggest that patients whose tumors express moderate to high MET levels could potentially benefit from METxMET-M114 treatment, even in the absence of gene amplification.

Next, we compared the effects of METxMET-M114 and the comparator MET ADC in tumor xenograft models. In Hs746T tumors, METxMET-M114 was significantly more effective than Comp-MMAE at the 3 mg/kg dose, while both ADCs promoted complete tumor regression at 10 mg/kg (**Fig. 3A**). In a *MET*-amplified NSCLC PDX model, METxMET-M114 was significantly more effective than Comp-MMAE at both 3 and 10 mg/kg (**Fig. 3B**). Finally, while METxMET-M114 at 5 mg/kg provided complete and durable regression of NCI-H441 tumors, Comp-MMAE promoted only transient tumor regression (**Fig. 2D**, left panel).

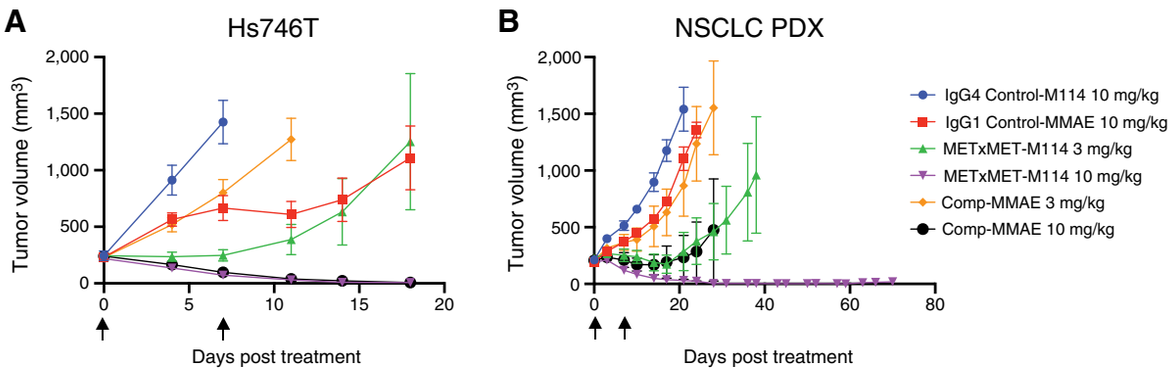

Figure 3.

METxMET-M114 compares favorably to a clinical-stage MET ADC. **A** and **B,** SCID mice bearing established Hs746T tumors or nude mice implanted with patient-derived tumor fragments were randomized ($n = 6$/group) and treated with ADCs at the indicated doses. ADC administrations are indicated by arrows. Line graphs depict the average tumor volumes ± SEM for each group.

METxMET ADC overcomes resistance to MET pathway inhibition

MET-selective TKIs have shown impressive activity in patients with *MET*-altered cancer (1, 2). However, as observed with other targeted therapies, resistance often limits the benefit of these agents (14–18). Thus, we tested the activity of METxMET-M114 in *MET*-altered models in which the response to MET pathway blockade is suboptimal, either because of inherent or acquired resistance. In *MET*-amplified/*MET*-ex14 Hs746T xenografts, our unconjugated METxMET antibody promotes complete tumor regression (**Fig. 4A**). However, the tumors eventually regrow, even in the continued presence of METxMET antibody. While METxMET antibody promotes MET degradation and a dramatic decrease in phospho-MET levels at 48 hours after initial treatment (**Fig. 4B**), the pathway appears to be reactivated in escaping tumors, that is, total and phospho-MET levels are similar in end-of-study tumors treated with either control or METxMET antibody. Importantly, treatment of escaping tumors with METxMET-M114 resulted in complete and durable regression, consistent with the continued expression of MET protein (**Fig. 4A**, green curve). Thus, as long as MET expression is maintained, METxMET-M114 may provide effective treatment of tumors in which the pathway has been reactivated despite the presence of a MET signaling blocker.

Innate resistance of *MET*-altered tumors due to activation of additional oncogenic drivers (e.g., KRAS) can also limit the benefit of MET-targeted therapies (17, 18). Relevant to this concept, treatment of a *MET*-amplified NSCLC PDX model with the unconjugated METxMET antibody only delayed tumor growth (**Fig. 4C**), presumably reflecting cancer cell proliferation driven by alternate signaling pathways. Consistent with that possibility, METxMET antibody significantly decreased the levels of total and phospho-MET in tumors, but failed to block MAPK signaling, indicating that another upstream pathway maintains MAP kinase activation when MET is blocked (**Fig. 4D**). In contrast to the modest effect of MET pathway blockade, METxMET-M114 promoted complete tumor regression of this PDX tumor, consistent with the high level of MET expressed in this model (**Fig. 4C**). Thus, METxMET-M114 may be an attractive alternative to targeted therapy in clinical settings where MET is a relatively weak driver because of cooccurring oncogenic alterations.

One strategy to overcome innate tumor resistance is to employ combinations of targeted agents. In lung cancer, MET and EGFR can functionally substitute for each other (1, 2), presumably because they signal through similar downstream pathways. For example, the *MET*-amplified lung cancer cell line EBC1 is primarily MET-driven, although EGFR blockade does modestly inhibit growth and the combined blockade of MET plus EGFR is more effective than either monotherapy (39, 40). Further, resistance of EBC1 cells to MET blockers can arise through a "switch" to EGFR signaling (39, 41). To compare the therapeutic effect of combined MET plus EGFR blockade to that of our METxMET ADC, EBC1 xenografts were treated with unconjugated METxMET antibody, an EGFR blocking antibody (in-house version of cetuximab), the combination of METxMET plus EGFR antibodies or METxMET-M114. While the MET plus EGFR combination treatment was more effective than METxMET antibody alone, only METxMET-M114 was able to induce complete tumor regression (**Fig. 4E**). These findings provide further support for the notion that a MET ADC may provide an effective means to overcome innate resistance to MET pathway blockade, and may compare favorably even to combinations of targeted therapies.

To investigate the activity of our METxMET ADC in a setting of MET TKI resistance, EBC1 cells were exposed to gradually increasing concentrations of capmatinib. As shown in **Fig. 4F**, the surviving cells (EBC1-CapR) were resistant to both capmatinib and to unconjugated METxMET antibody, suggesting an "off-target" mechanism of resistance. In contrast, the capmatinib-resistant cells remained highly sensitive to METxMET-M114 treatment. Although unconjugated METxMET antibody did not affect the viability of the capmatinib-resistant cells, it significantly reduced the levels of total and phosphorylated MET (**Fig. 4G**). However, METxMET antibody failed to completely block phosphorylation of MAPK, suggesting that EBC1-CapR cells have activated a bypass pathway that drives tumor cell growth when MET signaling is inhibited. Thus, in this particular case, acquired resistance to capmatinib cannot be overcome by switching to a distinct MET blocker, but our METxMET ADC maintains potent anti-tumor activity.

Immuno-PET imaging demonstrates tumor targeting of METxMET antibody

Because MET expression is a key determinant of METxMET ADC efficacy, accurate assessment of MET protein levels in tumors is an important aspect of a clinical development plan. PET imaging of radiolabeled METxMET antibody could provide a noninvasive method to assess MET expression over time and in different lesions, potentially helping to guide patient selection. To determine the biodistribution and tumor targeting of ^{89}Zr-METxMET in tumor xenografts, mice were administered 0.1 mg/kg of radiolabeled

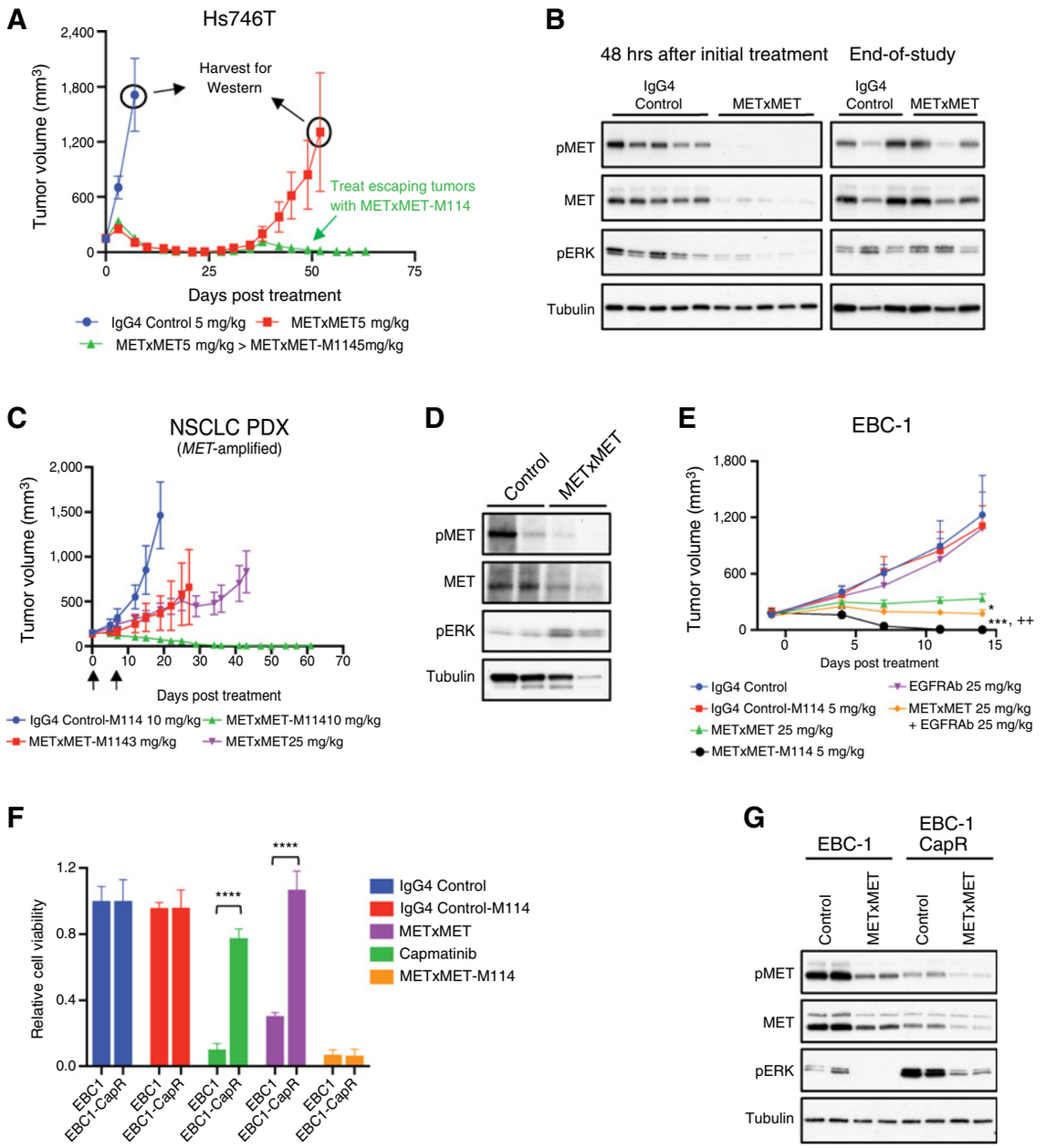

Figure 4.

METxMET ADC overcomes innate or acquired resistance to MET pathway inhibition. **A,** SCID mice bearing established Hs746T tumors were randomized ($n = 6$/group) and treated twice per week with IgG4 control or unconjugated METxMET antibody at 5 mg/kg. Escaping tumors either continued to receive unconjugated METxMET antibody (red curve) or were switched to 5 mg/kg of METxMET-M114, administered on days 38 and 45 (green curve). Line graphs depict the average tumor volumes ± SEM for each group. **B,** Western blots showing the levels of the indicated proteins in Hs746T tumors (shown in **A**) treated with control IgG4 or unconjugated METxMET antibody. Tumors were harvested either at 48 hours after the initiation of antibody treatment or at the end of the study. **C,** Nude mice bearing established NSCLC PDX were randomized ($n = 6$/group) and treated with the indicated ADCs or unconjugated METxMET antibody at the indicated doses. ADCs were administered on days 0 and 7. Unconjugated METxMET antibody was administered twice per week. **D,** Western blots showing the levels of the indicated proteins in PDX tumors (shown in **C**) treated with control IgG4 or unconjugated METxMET antibody. Tumors were harvested at the end of the study. **E,** SCID mice bearing established EBC1 tumors were randomized ($n = 5$/group) and treated with the indicated unconjugated antibodies or ADCs. Unconjugated antibodies were administered twice per week. ADCs were administered on day 0. *, $P < 0.05$; ***, $P < 0.0005$ versus METxMET, ++$P < 0.005$ versus METxMET + EGFR Ab. **F,** EBC1 parental or capmatinib-resistant (CapR) cells were treated with the indicated agents and cell viability was measured after 5 days. Unconjugated antibodies were administered twice at 5 μg/mL. ADCs (5 μg/mL) and capmatinib (25 nmol/L) were administered once. The bar graph depicts the relative cell viability in each treatment group (mean ± SD). ****, $P < 0.0001$, one-way ANOVA with Tukey *post hoc* test. **G,** Western blots showing the levels of the indicated proteins in EBC1 parental or capmatinib-resistant cells treated with IgG4 control or unconjugated METxMET antibody at 5 μg/mL for 18 hours.

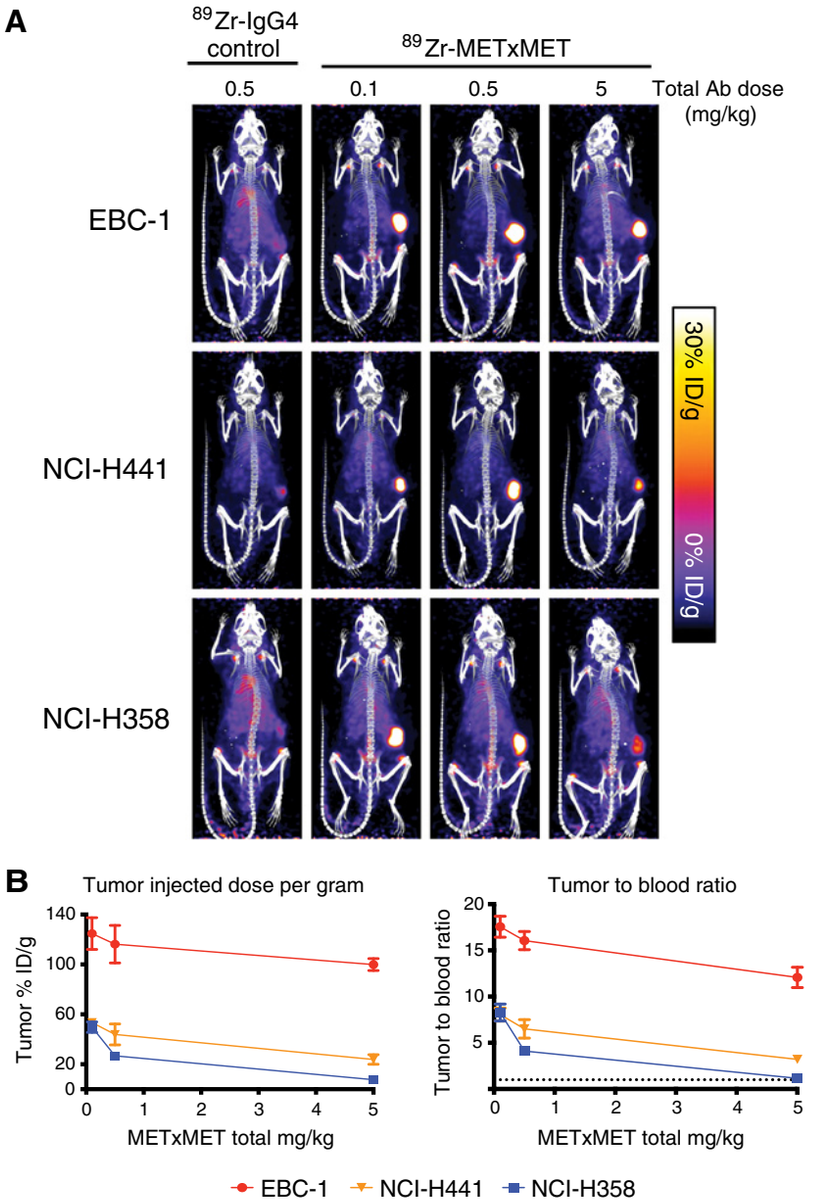

Figure 5.

Immuno-PET imaging demonstrates tumor targeting of METxMET antibody. **A,** Representative images from mice bearing established tumors (right flank) 6 days after administration of ^{89}Zr-radiolabeled control or METxMET antibody (0.1 mg/kg). In some groups, mice received unlabeled METxMET antibody to bring the total antibody dose up to 0.5 or 5 mg/kg, as indicated. **B,** Quantitative *ex vivo* biodistribution was performed on day 6 post injection. The line graphs depict radioactivity in the tumor or tumor to blood ratio expressed as percentage injected dose per gram of tissue (%ID/g).

METxMET antibody along with increasing concentrations of unlabeled METxMET antibody. ^{89}Zr-METxMET was localized specifically to the tumors at 6 days after administration, and the degree of uptake was greater in EBC1 tumors than in NCI-H441 or NCI-H358 tumors (**Fig. 5A**). Uptake of ^{89}Zr-METxMET in NCI-H358 tumors, which express lower levels of MET (Supplementary Fig. S1), was reduced at higher doses of unlabeled antibody compared with NCI-H441 or EBC1 tumors (**Fig. 5B**), suggesting competition between labeled and unlabeled antibody for binding to available receptor. Thus, it may be possible to establish a relationship between uptake of ^{89}Zr-METxMET in tumors and responsiveness to METxMET-M114 treatment.

METxMET-M114 exhibits a favorable toxicity profile in cynomolgus monkeys

The ability of METxMET-M114 to bind cynomolgus monkey MET (Supplementary Table S3) allowed us to conduct a repeat-dose toxicology study to characterize its pharmacokinetics, safety, and tolerability. Control IgG4-M114 or METxMET-M114 were administered intravenously at 10 mg/kg to cynomolgus monkeys on day 1 and again on day 22. At the completion of dosing, two animals from each group were euthanized and tissues were examined for microscopic findings. The remaining animals were evaluated for reversibility of any test article-related effects during a 6-week recovery phase. METxMET-M114 was well tolerated with no test article-related clinical observations evident during the dosing or recovery phase.

Concentration–time profiles for total and conjugated METxMET antibody in serum revealed that the exposures of the total antibody and conjugated antibody analytes were similar when comparing both C_{max} and AUC values (**Fig. 6A**; Supplementary Table S4). The ratio of conjugated antibody/total antibody AUC_{last} values following the first dose was approximately 78%, indicating that most of the METxMET antibody remains conjugated over the dosing interval. Mean terminal

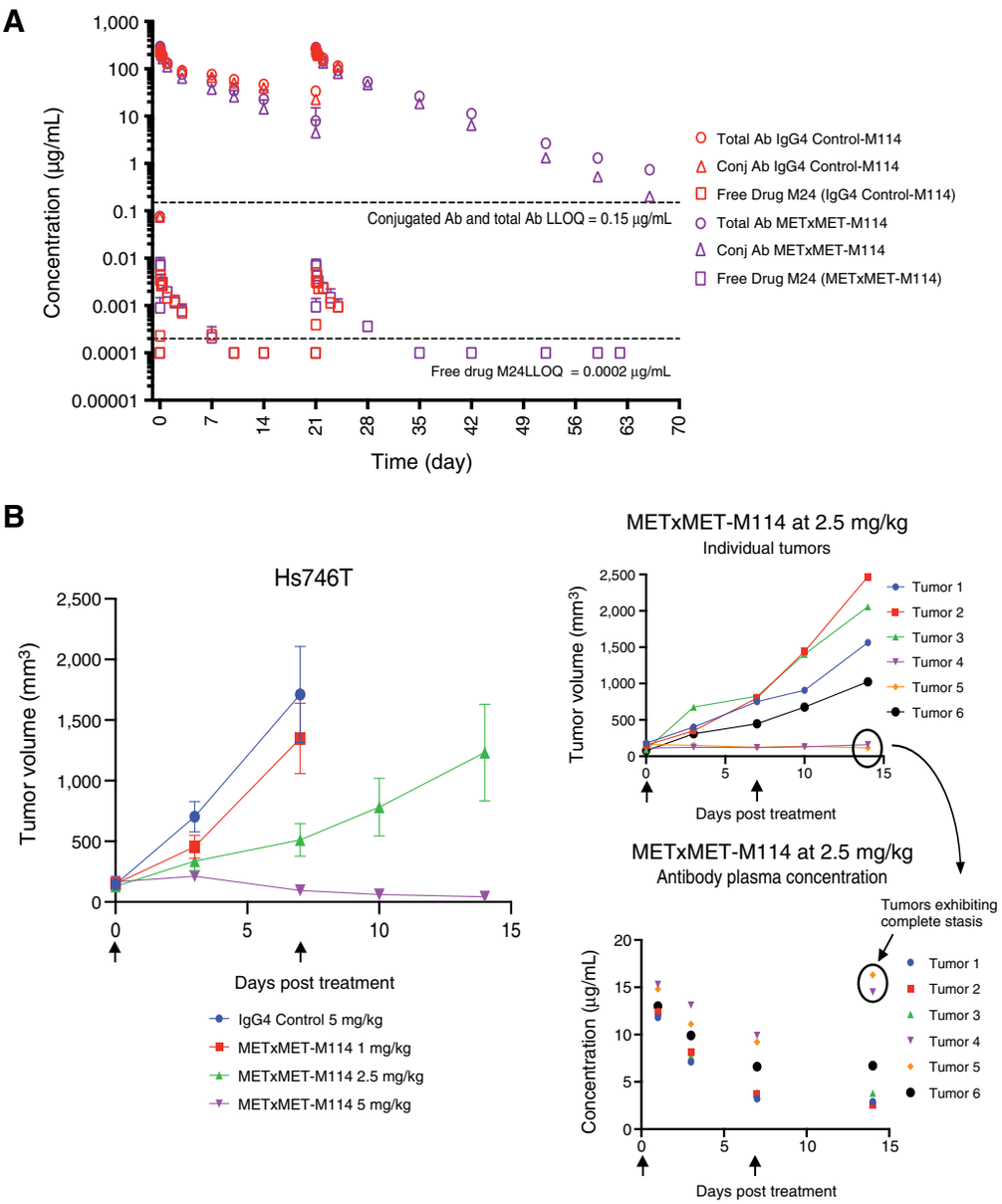

Figure 6.

METxMET-M114 exhibits a favorable toxicity profile in cynomolgus monkeys. **A,** Male and female cynomolgus monkeys (n = 4/group) were administered IgG4 control-M114 or METxMET-M114 into the saphenous vein on days 1 and 22. Blood samples were collected for evaluation of total antibody, conjugated antibody, and free payload M24 concentration using antigen-specific immunoassays or mass spectrometry. LLOQ; lower limit of quantitation. **B,** SCID mice bearing Hs746T tumors (n = 6/group) were randomized and treated with IgG4 control-M114 or METxMET-M114 at the indicated doses on days 0 and 7 (indicated by arrows). Line graphs depict the average tumor volumes ± SEM for each group (left) or individual tumors treated with 2.5 mg/kg METxMET-M114 (top right). The bottom right panel shows the total antibody plasma concentrations in each mouse. Plasma was collected on days 3, 7 (pre dose), 10, and 14.

half-life values ranged from 4.0–5.1 days for total METxMET antibody and 3.3–4.5 days for conjugated METxMET antibody, respectively. Concentrations of free payload M24 in plasma were very low compared with total Ab or conjugated Ab, and were similar for the control ADC and METxMET-M114 groups (**Fig. 6A**; Supplementary Table S4).

To investigate the relationship between METxMET-M114 concentration in plasma and antitumor efficacy, Hs746T tumor-bearing mice were treated with 1 to 5 mg/kg of METxMET-M114 and circulating human IgG pharmacokinetic parameters were measured. Tumor growth delay or regression was observed at the 2.5 or 5 mg/kg doses, respectively (**Fig. 6B**). In mice receiving 2.5 mg/kg of METxMET-M114, two tumors exhibited complete stasis, a response that was associated with trough antibody concentrations of approximately 8 µg/mL following the first administration of ADC and 16 µg/mL following the second administration (**Fig. 6B**). Thus, dosing regimens

of METxMET-M114 that achieve minimum plasma concentrations of approximately 10 μg/mL result in complete tumor growth inhibition. Importantly, the concentration of circulating METxMET-M114 in cynomolgus monkeys exceeded this value for at least two weeks following administration of a 10 mg/kg dose (which was very well tolerated). Thus, METxMET-M114 is potentially an attractive therapy for MET-overexpressing cancers.

Discussion

In this report, we have characterized the properties of a novel biparatopic ADC, METxMET-M114, which is highly effective in MET-expressing tumor models regardless of pathway dependence, including *MET*-altered models that are resistant to inhibition of MET signaling. Our findings suggest that METxMET-M114 is a promising candidate for the treatment of MET-expressing tumors, with the potential to address some of the limitations faced by MET blockers.

The MET ADC telisotuzumab vedotin has provided preliminary validation of MET as an ADC target. This agent is well tolerated, with adverse events that appear to be payload-driven, and has exhibited signs of antitumor activity (20, 42). However, response data are available from only a small number of treated patients and the optimal dosing regimen and inclusion criteria (i.e., IHC cutoff) are apparently still under investigation (42). Thus, the magnitude of the benefit that telisotuzumab vedotin will provide to patients with NSCLC remains to be determined.

As shown previously (23), our biparatopic METxMET antibody (known as REGN5093 and now in a phase I clinical trial) internalizes rapidly and traffics efficiently to lysosomes, ideal characteristics for the antibody component of an ADC. These functional properties of our METxMET antibody may reflect the fact that it forms a 2:2 antibody/MET complex, rather than the 1:2 complex typical of conventional antibodies. This larger complex recycles inefficiently, resulting in lysosomal trafficking and MET degradation (23). Interestingly, two biparatopic ADCs targeting HER2 (MEDI4276 and ZW49) have entered the clinic (43, 44). While we have not directly compared the trafficking properties of these ADCs to our MET ADC, published data indicate that the biparatopic HER2 ADCs also traffic very efficiently to lysosomes.

METxMET-M114 employs a protease-cleavable linker, which could mean less susceptibility to ADC resistance mechanisms such as reduced lysosomal proteolysis (45). An additional design consideration was the use of a payload with poor cell permeability (24), resulting in an ADC that is very unlikely to possess significant bystander killing activity. Given that MET is expressed in several normal tissues, the lack of bystander killing may be a favorable property from a tolerability perspective.

In addition to treating tumors that are resistant to MET TKIs, METxMET-M114 might be an attractive option in settings where *MET* amplification drives resistance to EGFR TKIs (*MET* amplification may account for up to 15%–20% of resistance to third-generation EGFR TKIs (46, 47)). While the combination of MET plus EGFR TKIs provides benefit in this setting (7–9), such combination regimens may not be very well tolerated (8).

In summary, our data show that METxMET-M114 has potent antitumor activity and a favorable preclinical safety profile, supporting the clinical evaluation of this novel agent in MET-expressing cancers.

Authors' Disclosures

J.O. DaSilva reports a patent for US2018/0134794A1 issued to Regeneron Pharmaceuticals, Inc. O. Surriga reports personal fees from Columbia University Irving Medical Center and personal fees from Pfizer outside the submitted work. T. Nittoli reports a patent for US10570151 issued to Regeneron and a patent for US 20180134794 pending. M.C. Franklin is a stockholder in and employee of Regeneron Pharmaceuticals, Inc., which is developing the molecules described in this manuscript as potential marketed therapies. G. Thurston is an employee and shareholder of Regeneron Pharmaceuticals. C. Daly reports a patent for anti-MET antibodies, bispecific antigen binding molecules that bind MET, and methods of use thereof pending to Regeneron Pharmaceuticals, Inc. No disclosures were reported by the other authors.

Authors' Contributions

J.O. DaSilva: Conceptualization, data curation, formal analysis, supervision, writing–original draft, project administration, writing–review and editing. **K. Yang:** Investigation. **O. Surriga:** Investigation. **T. Nittoli:** Resources, data curation, supervision, project administration. **A. Kunz:** Investigation. **M.C. Franklin:** Investigation. **F.J. Delfino:** Resources, investigation, methodology. **S. Mao:** Investigation. **F. Zhao:** Investigation. **J.T. Giurleo:** Resources, investigation, methodology. **M.P. Kelly:** Investigation, methodology. **S. Makonnen:** Investigation. **C. Hickey:** Investigation. **P. Krueger:** Investigation, methodology. **R. Foster:** Investigation. **Z. Chen:** Investigation. **M.W. Retter:** Formal analysis, investigation, methodology. **R. Slim:** Formal analysis, investigation. **T.M. Young:** Investigation, methodology. **W.C. Olson:** Formal analysis, supervision. **G. Thurston:** Formal analysis, supervision. **C. Daly:** Conceptualization, formal analysis, supervision, writing–original draft, project administration, writing–review and editing.

Acknowledgments

The authors thank F. Barletta for pharmacokinetic analysis, C. Castanaro for helpful comments and suggestions, and all Regeneron employees who contributed to the generation of the antibody–drug conjugates used in this study.

The costs of publication of this article were defrayed in part by the payment of page charges. This article must therefore be hereby marked *advertisement* in accordance with 18 U.S.C. Section 1734 solely to indicate this fact.

Received January 5, 2021; revised March 30, 2021; accepted June 14, 2021; published first July 26, 2021.

References

1. Guo R, Luo J, Chang J, Rekhtman N, Arcila M, Drilon A. MET-dependent solid tumours - molecular diagnosis and targeted therapy. Nat Rev Clin Oncol 2020; 17:569–87.
2. Recondo G, Che J, Jänne PA, Awad MM. Targeting MET dysregulation in cancer. Cancer Discov 2020;10:922–34.
3. Comoglio PM, Trusolino L, Boccaccio C. Known and novel roles of the MET oncogene in cancer: a coherent approach to targeted therapy. Nat Rev Cancer 2018;18:341–58.
4. Paik PK, Felip E, Veillon R, Sakai H, Cortot AB, Garassino MC, et al. Tepotinib in non-small-cell lung cancer with MET exon 14 skipping mutations. N Engl J Med 2020;383:931–43.
5. Wolf J, Seto T, Han J-Y, Reguart N, Garon EB, Groen HJM, et al. Capmatinib in MET exon 14-mutated or MET-amplified non-small-cell lung cancer. N Engl J Med 2020;383:944–57.
6. Drilon A, Clark JW, Weiss J, Ou S-HI, Camidge DR, Solomon BJ, et al. Antitumor activity of crizotinib in lung cancers harboring a MET exon 14 alteration. Nat Med 2020;26:47–51.
7. Oxnard GR, Yang JC-H, Yu H, Kim S-W, Saka H, Horn L, et al. TATTON: a multi-arm, phase Ib trial of osimertinib combined with selumetinib, savolitinib, or durvalumab in EGFR-mutant lung cancer. Ann Oncol 2020;31:507–16.
8. Sequist LV, Han J-Y, Ahn M-J, Cho BC, Yu H, Kim S-W, et al. Osimertinib plus savolitinib in patients with EGFR mutation-positive, MET-amplified,

non-small-cell lung cancer after progression on EGFR tyrosine kinase inhibitors: interim results from a multicentre, open-label, phase 1b study. Lancet Oncol 2020;21:373–86.
9. Wu Y-L, Zhang L, Kim D-W, Liu X, Lee DH, Yang JC-H, et al. Phase Ib/II study of capmatinib (INC280) plus gefitinib after failure of epidermal growth factor receptor (EGFR) inhibitor therapy in patients with EGFR-mutated, MET factor-dysregulated non-small-cell lung cancer. J Clin Oncol 2018;36:3101–9.
10. An X, Wang F, Shao Q, Wang F-H, Wang Z-Q, Chen C, et al. MET amplification is not rare and predicts unfavorable clinical outcomes in patients with recurrent/metastatic gastric cancer after chemotherapy. Cancer 2014;120:675–82.
11. Koeppen H, Yu W, Zha J, Pandita A, Penuel E, Rangell L, et al. Biomarker analyses from a placebo-controlled phase II study evaluating erlotinib+/-onartuzumab in advanced non-small cell lung cancer: MET expression levels are predictive of patient benefit. Clin Cancer Res 2014;20:4488–98.
12. Reis H, Metzenmacher M, Goetz M, Savvidou N, Darwiche K, Aigner C, et al. MET expression in advanced non-small-cell lung cancer: effect on clinical outcomes of chemotherapy, targeted therapy, and immunotherapy. Clin Lung Cancer 2018;19:e441–63.
13. Casadevall D, Gimeno J, Clavé S, Taus Á, Pijuan L, Arumí M, et al. MET expression and copy number heterogeneity in nonsquamous non-small cell lung cancer (nsNSCLC). Oncotarget 2015;6:16215–26.
14. Bahcall M, Awad MM, Sholl LM, Wilson FH, Xu M, Wang S, et al. Amplification of wild-type KRAS imparts resistance to crizotinib in MET exon 14 mutant non-small cell lung cancer. Clin Cancer Res 2018;24:5963–76.
15. Guo R, Offin M, Brannon AR, Chow A, Delasos L, Somwar R, et al. MET inhibitor resistance in patients with MET exon 14-altered lung cancers. J Clin Oncol 2019;37(suppl; abstr 9006).
16. Recondo G, Bahcall M, Spurr LF, Che J, Ricciuti B, Leonardi GC, et al. Molecular mechanisms of acquired resistance to MET tyrosine kinase inhibitors in patients with MET exon 14-mutant NSCLC. Clin Cancer Res 2020;26:2615–25.
17. Rotow JK, Gui P, Wu W, Raymond VM, Lanman RB, Kaye FJ, et al. Co-occurring alterations in the RAS-MAPK pathway limit response to MET inhibitor treatment in MET exon 14 skipping mutation-positive lung cancer. Clin Cancer Res 2020;26:439–49.
18. Suzawa K, Offin M, Lu D, Kurzatkowski C, Vojnic M, Smith RS, et al. Activation of KRAS mediates resistance to targeted therapy in MET exon 14-mutant non-small cell lung cancer. Clin Cancer Res 2019;25:1248–60.
19. Gymnopoulos M, Betancourt O, Blot V, Fujita R, Galvan D, Lieuw V, et al. TR1801-ADC: a highly potent cMet antibody-drug conjugate with high activity in patient-derived xenograft models of solid tumors. Mol Oncol 2020;14:54–68.
20. Strickler JH, Weekes CD, Nemunaitis J, Ramanathan RK, Heist RS, Morgensztern D, et al. First-in-human phase I, dose-escalation and -expansion study of telisotuzumab vedotin, an antibody-drug conjugate targeting c-Met, in patients with advanced solid tumors. J Clin Oncol 2018;36:3298–306.
21. Wang J, Anderson MG, Oleksijew A, Vaidya KS, Boghaert ER, Tucker L, et al. ABBV-399, a c-Met antibody-drug conjugate that targets both MET-amplified and c-Met-overexpressing tumors, irrespective of MET pathway dependence. Clin Cancer Res 2017;23:992–1000.
22. Yang C-Y, Wang L, Sun X, Tang M, Quan H-T, Zhang L-S, et al. SHR-A1403, a novel c-Met antibody-drug conjugate, exerts encouraging anti-tumor activity in c-Met-overexpressing models. Acta Pharmacol Sin 2019;40:971–9.
23. DaSilva JO, Yang K, Perez Bay AE, Andreev J, Ngoi P, Pyles E, et al. A biparatopic antibody that modulates MET trafficking exhibits enhanced efficacy compared with parental antibodies in MET-driven tumor models. Clin Cancer Res 2020;26:1408–19.
24. Nittoli T, Kelly MP, Delfino F, Rudge J, Kunz A, Markotan T, et al. Antibody drug conjugates of cleavable amino-alkyl and aryl maytansinoids. Bioorg Med Chem 2018;26:2271–9.
25. Zhang L, Castanaro C, Luan B, Yang K, Fan L, Fairhurst JL, et al. ERBB3/HER2 signaling promotes resistance to EGFR blockade in head and neck and colorectal cancer models. Mol Cancer Ther 2014;13:1345–55.
26. Murphy AJ, Macdonald LE, Stevens S, Karow M, Dore AT, Pobursky K, et al. Mice with megabase humanization of their immunoglobulin genes generate antibodies as efficiently as normal mice. Proc Natl Acad Sci U S A 2014;111:5153–8.
27. Babb R, Chen G, Daly C, DaSilva J, MacDonald D, inventors; Regeneron Pharmaceuticals, Inc, assignee. Anti-MET antibodies, bispecific antigen binding molecules that bind MET, and methods of use therof.
28. Smith EJ, Olson K, Haber LJ, Varghese B, Duramad P, Tustian AD, et al. A novel, native-format bispecific antibody triggering T-cell killing of B-cells is robustly active in mouse tumor models and cynomolgus monkeys. Sci Rep 2015;5:17943.
29. Hamblett KJ, Senter PD, Chace DF, Sun MMC, Lenox J, Cerveny CG, et al. Effects of drug loading on the antitumor activity of a monoclonal antibody drug conjugate. Clin Cancer Res 2004;10:7063–70.
30. Prota AE, Magiera MM, Kuijpers M, Bargsten K, Frey D, Wieser M, et al. Structural basis of tubulin tyrosination by tubulin tyrosine ligase. J Cell Biol 2013;200:259–70.
31. Emsley P, Lohkamp B, Scott WG, Cowtan K. Features and development of Coot. Acta Crystallogr D Biol Crystallogr 2010;66:486–501.
32. Murshudov GN, Skubák P, Lebedev AA, Pannu NS, Steiner RA, Nicholls RA, et al. REFMAC5 for the refinement of macromolecular crystal structures. Acta Crystallogr D Biol Crystallogr, 2011;67:355–67.
33. Vosjan MJWD, Perk LR, Visser GWM, Budde M, Jurek P, Kiefer GE, et al. Conjugation and radiolabeling of monoclonal antibodies with zirconium-89 for PET imaging using the bifunctional chelate p-isothiocyanatobenzyl-desferrioxamine. Nat Protoc 2010;5:739–43.
34. Prota AE, Bargsten K, Diaz JF, Marsh M, Cuevas C, Liniger M, et al. A new tubulin-binding site and pharmacophore for microtubule-destabilizing anticancer drugs. Proc Natl Acad Sci U S A 2014;111:13817–21.
35. Basilico C, Pennacchietti S, Vigna E, Chiriaco C, Arena S, Bardelli A, et al. Tivantinib (ARQ197) displays cytotoxic activity that is independent of its ability to bind MET. Clin Cancer Res 2013;19:2381–92.
36. Kubo T, Yamamoto H, Lockwood WW, Valencia I, Soh J, Peyton M, et al. MET gene amplification or EGFR mutation activate MET in lung cancers untreated with EGFR tyrosine kinase inhibitors. Int J Cancer 2009;124:1778–84.
37. Hamblett KJ, Jacob AP, Gurgel JL, Tometsko ME, Rock BM, Patel SK, et al. SLC46A3 is required to transport catabolites of noncleavable antibody maytansine conjugates from the lysosome to the cytoplasm. Cancer Res 2015;75:5329–40.
38. Kinneer K, Meekin J, Tiberghien AC, Tai Y-T, Phipps S, Kiefer CM, et al. SLC46A3 as a potential predictive biomarker for antibody-drug conjugates bearing noncleavable linked maytansinoid and pyrrolobenzodiazepine warheads. Clin Cancer Res 2018;24:6570–82.
39. McDermott U, Pusapati RV, Christensen JG, Gray NS, Settleman J. Acquired resistance of non-small cell lung cancer cells to MET kinase inhibition is mediated by a switch to epidermal growth factor receptor dependency. Cancer Res 2010;70:1625–34.
40. Zhang Y-W, Staal B, Essenburg C, Lewis S, Kaufman D, Vande Woude GF. Strengthening context-dependent anticancer effects on non-small cell lung carcinoma by inhibition of both MET and EGFR. Mol Cancer Ther 2013;12:1429–41.
41. Kim S, Kim TM, Kim D-W, Kim S, Kim M, Ahn Y-O, et al. Acquired resistance of MET-amplified non-small cell lung cancer cells to the MET inhibitor capmatinib. Cancer Res Treat 2019;51:951–62.
42. Heist RS, Motwani M, Barlesi F, Goldman JW, Kelly K, Sun Y, et al. c-Met expression and response to telisotuzumab vedotin (teliso-v) in patients with non-small cell lung cancer. J Clin Oncol 2019;37:9023.
43. Li JY, Perry SR, Muniz-Medina V, Wang X, Wetzel LK, Rebelatto MC, et al. A biparatopic HER2-targeting antibody-drug conjugate induces tumor regression in primary models refractory to or ineligible for HER2-targeted therapy. Cancer Cell 2016;29:117–29.
44. Hamblett KJ, Barnscher SD, Davies RH, Hammond PW, Hernandez A, Wickman GR, et al. ZW49, a HER2 targeted biparatopic antibody drug conjugate for the treatment of HER2 expressing cancers [abstract]. In: Proceedings of the 2018 San Antonio Breast Cancer Symposium; 2018 Dec 4-8; San Antonio, TX. Philadelphia (PA): AACR; Cancer Res 2019;79(4 Suppl):Abstract nr P6-17-13.
45. Ríos-Luci C, García-Alonso S, Díaz-Rodríguez E, Nadal-Serrano M, Arribas J, Ocaña A, et al. Resistance to the antibody-drug conjugate T-DM1 is based in a reduction in lysosomal proteolytic activity. Cancer Res 2017;77:4639–51.
46. Chabon JJ, Simmons AD, Lovejoy AF, Esfahani MS, Newman AM, Haringsma HJ, et al. Circulating tumour DNA profiling reveals heterogeneity of EGFR inhibitor resistance mechanisms in lung cancer patients. Nat Commun 2016;7:11815.
47. Piper-Vallillo AJ, Sequist LV, Piotrowska Z. Emerging treatment paradigms for EGFR-mutant lung cancers progressing on osimertinib: a review. J Clin Oncol 2020;38:2926–36.